Analytical approach for the use of different gauges in bubble wakefield acceleration

Sonu Kumar[1], Vidushi Dhaka[2], Hitendra K. Malik[1]*, Dhananjay K. Singh[3]

Abstract
Laser and plasma interaction leads to several fascinating nonlinear phenomena, out of which bubble wakefield excitation is one of the recent interests. This field is used for the particle acceleration, which is very useful for high energy physics, betatron radiation emission, cancer therapy, etc. In the present work, an electromagnetic field is evaluated in bubble wakefield regime and the shape of the bubble is shown to be controlled by d'Alembert differential equations and different Gauge conditions. Wakefield potential is calculated in different bubble regimes such as spherical, longitudinal ellipsoid, transverse ellipsoid bubble regimes. A geometrical parameter is found to decide the size of the bubble. A detailed study of the same is conducted under the effect of different electron residual density. A comparative study of different Gauge conditions shows that the accelerator gradient is maximum in transverse ellipsoid bubble case. Also, energy gain in dephasing length is evaluated that shows maximum energy when bubble assumes transverse ellipsoid shape.

Keywords
Bubble regime, bubble wakefield acceleration, dephasing length, wakefield, geometrical parameter, d'Alembert differential equations.

[1] *Plasma Waves and Particle Acceleration Laboratory, Department of Physics, Indian Institute of Technology Delhi, New Delhi - 110016, India*
[2] *Springdale College, Surbhi Colony, Madhotanda Road, Pilibhit, Uttar Pradesh – 262001, India*
[3] *Department of Physics, PKRM College, Dhanbad - 826004, Jharkhand, India*
*Corresponding author: hkmalik@hotmail.com

1. Introduction

Bubble wakefield acceleration is a new concept for acceleration of charged particles in laser wakefield acceleration first given by Tajima and Dawson in 1979 [1]. In bubble wakefield acceleration, an intense short laser pulse excites all the plasma electrons and expells them, forming an ion cavity behind the laser pulse [2–6]. Expelled electrons create an electron sheath around bubble boundary, but these electrons move back to their position due to ions and overshoot their initial positions due to their momentum and create an electron plasma wave called wake. The electrons can be self-trapped, and accelerated otherwise externally injected electrons are accelerate to high energy [7, 8]. In laser Wakefield acceleration, the observation of formation of bubble has been made by Hakimi et al. [9]. Advantage of this bubble formation [10] and self – injection [11, 12] of trapped electrons is that there is no need of external bunch of electrons as witness bunch and self -production is possible [13]. In sub-terawatt laser Wakefield acceleration, ionization-induced injection's simulation investigation has been made by Lin et al. [14]. In a sub-mm nitrogen gas jet, Lin et al. [15] have analyzed a few-terawatt laser pulse driven laser Wakefield acceleration. For mid-IR laser drivers in the bubble regime, laser Wakefield acceleration has been studied by Woodbury et al. [16]. Through angular distributions of betatron x-rays in laser Wakefield accelera-

tion, diagnosis of bubble evolution has been done by Ma et al. [17]. This acceleration technique is very useful for high energy physics, betatron radiation emission, cancer therapy and renewable clean energy and many more [18–20].

Kostyukov et al. [21] and Wu et al. [22] have developed models for spherical bubble regime for bubble wakefield acceleration and, these do not talk about the modification of bubble shape but Sadighi-Bonabi and Rahmatollapur [23] and Li et al. [24] have used such concept and found different bubble shapes called longitudinal ellipsoid and transverse ellipsoid bubbles. They have evaluated the corresponding electromagnetic fields.

To the best of our knowledge, no investigation has been so far done for the calculations of accelerator gradient and maximum energy gain in different shaped bubble regimes. We have developed theoretical model for different shaped bubble regimes and energy gain in dephasing length. In addition, we have considered different gauge conditions for evaluating the acceleration gradient and maximum energy.

1.1 Dephasing length in bubble regime

When accelerated electrons outrun the plasma wave and decelerate, then the length of acceleration to deceleration region is called as dephasing length [25]. Dephasing length is different in different regimes. It is used to control energy gain in laser wakefield acceleration [26]. Here acceleration distance

is limited by dephasing length by [27].

In 3D nonlinear or bubble regime [28], the dephasing length is defined as:

$$L_d = \frac{c\lambda_p}{(c - v_{ph})} \tag{1}$$

where, λ_p is the plasma wavelength and v_{ph} is the phase velocity of the wakefield which is same as group velocity of the laser pulse. But, in bubble regime, group velocity of the laser pulse decreases due to pump depletion. In this depletion, laser pulse losses its energy due to etching velocity of the photons owing to its decrement being $v_{etch} = c\omega_p^2/\omega^2$. Therefore, the group velocity of the laser pulse which is equal to the phase velocity v_b of bubble.

$$v_g = c\sqrt{1 - \frac{\omega_p^2}{\omega^2}} - v_{etch} \tag{2}$$

For an underdense plasma, $\omega \gg \omega_p$, Hence

$$v_g = v_b = c\left(1 - \frac{3}{2}\frac{\omega_p^2}{\omega^2}\right) \tag{3}$$

$$L_d = \frac{2}{3}\frac{\omega^2}{\omega_p^2}\lambda_p = \frac{2}{3}\frac{\omega^2}{\omega_p^2}r_b \tag{4}$$

together with r_b as the radius of bubble wake. This is obtained by equating laser pulse ponderomotive force and electrostatic force of ion cavity on the wakefield electrons being $r_b = 2\sqrt{a_0}/k_p$ [11].

2. Analytical investigation

In laser-plasma interaction when the intensity of the laser is sufficiently high, laser pulse expels all the plasma electrons, creating an ion cavity generally spherical in shape. In the present work, we consider different geometrical bubble shapes with the help of d'Alembert differential equations and find energy gain in the bubble regime.

The d'Alembert differential equations are taken in terms of the electromagnetic field generated by the laser pulse inside plasma with the help of Maxwell's equations and scalar and vector potentials. Here we use Gaussian system of units. The dimensionless quantities are obtained by normalizing the length with k_p, velocity with $c = 3 \times 10^8$ m/s, $\mathbf{E}$ with $E_0 = m_e c\omega_p/e = 96$ GV/m, ϕ with $m_e c^2/e$, $\mathbf{A}$ with $m_e c^2/e.\phi$ and $\mathbf{A}$ being the scalar and vector potentials of the electromagnetic field, $\mathbf{J}$ and $\rho = (1 - n_a)$ are current and charge densities together with $\mathbf{J} = -en_a\mathbf{p}/\gamma_p$, where $\gamma_p = 1/\sqrt{1 - v_b^2/c^2}$, v_b is the phase velocity of bubble, ω is the laser frequency [26] and n_a is the residual electron density normalized by ambient plasma electrons density $n_0 = 10^{18}$ cm^{-3}. According to

Wu et al. $J_x = -en_a v_x$ and $\mathbf{J}_\perp = 0$ [22]. The laser pulse is considered to propagate in the x-direction creating an ion cavity. Here we follow Li et al. [24] and consider more Gauge conditions. $W_{max} = E_x L_d$ is the normalized energy gain, normalized with $m_e c^2$ [26] and bubble radius $r_b = 2\sqrt{a_0}$ which is obtained by equating laser pulse ponderomotive force and electrostatic force normalized with $r_0 = c/\omega_p$. . The plasma frequency $\omega_p = \sqrt{4\pi n_0 e^2/m_e} = 5.656 \times 10^{13}$ rad/s and dephasing length [25]

$$L_d = \frac{2\sqrt{a_0}}{3}\frac{\omega_0^2}{\omega_p^2} = \frac{2\sqrt{a_0}}{3}\gamma_p^2$$

We consider different Gauge conditions and wakefield potentials, defined as follows:

I. $A_x = \phi$ and generated wakefield potential $\Phi = A_x + \phi$

II. $\nabla_\perp.\mathbf{A}_\perp = -\frac{\partial\phi}{\partial\xi}$ and $\Phi = A_x - \phi$

III. $A_x = -\phi$ and generated wakefield potential $\Phi = A_x - \phi$

$\mathbf{A} = A - x\hat{x} + A_y\hat{y} + A_z\hat{z}$ is vector potential of electromagnetic field. The transverse component

$\mathbf{A}_\perp = A_y\hat{y} + A_z\hat{z}$

Maxwell's equations in normalized form can be written as:

$$\nabla.\mathbf{E} = 1 - n_a \tag{5}$$

$$\nabla.\mathbf{B} = 0 \tag{6}$$

$$\nabla \times \mathbf{E} = -\frac{\partial\mathbf{B}}{\partial t} \tag{7}$$

$$\nabla \times \mathbf{B} = \mathbf{J} + \frac{\partial\mathbf{E}}{\partial t} \tag{8}$$

$$\mathbf{E} = -\nabla\phi - \frac{\partial\mathbf{A}}{\partial t} \tag{9}$$

$$\mathbf{B} = \nabla \times \mathbf{A} \tag{10}$$

From 5 and 9,

$$\nabla.\left(-\nabla\phi - \frac{\partial\mathbf{A}}{\partial t}\right) = 1 - n_a \tag{11}$$

and from 8 and 10,

$$\nabla \times (\nabla \times \mathbf{A}) = \mathbf{J} + \frac{\partial}{\partial t}\left(-\nabla\phi - \frac{\partial\mathbf{A}}{\partial t}\right) \tag{12}$$

The above equations can be written as

$$\nabla^2\phi + \frac{\partial}{\partial t}\nabla.\mathbf{A} = -\rho = -(1 - n_a) \tag{13}$$

$$\nabla^2\mathbf{A} - \frac{\partial^2\mathbf{A}}{\partial t^2} - \nabla\left(\nabla.\mathbf{A} + \frac{\partial\phi}{\partial t}\right) = -\mathbf{J} \tag{14}$$
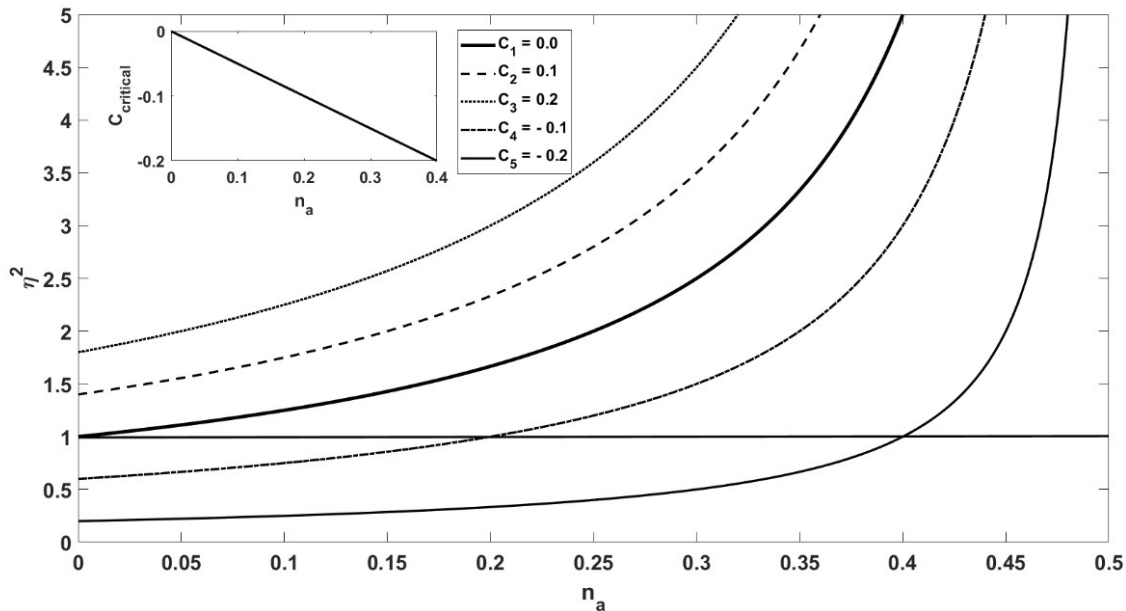
Figure 1. Variation of geometrical parameter η^2 along y-direction related to shape of bubble having residual electrons density n_a along x-direction with a change of transverse geometrical coefficient C.
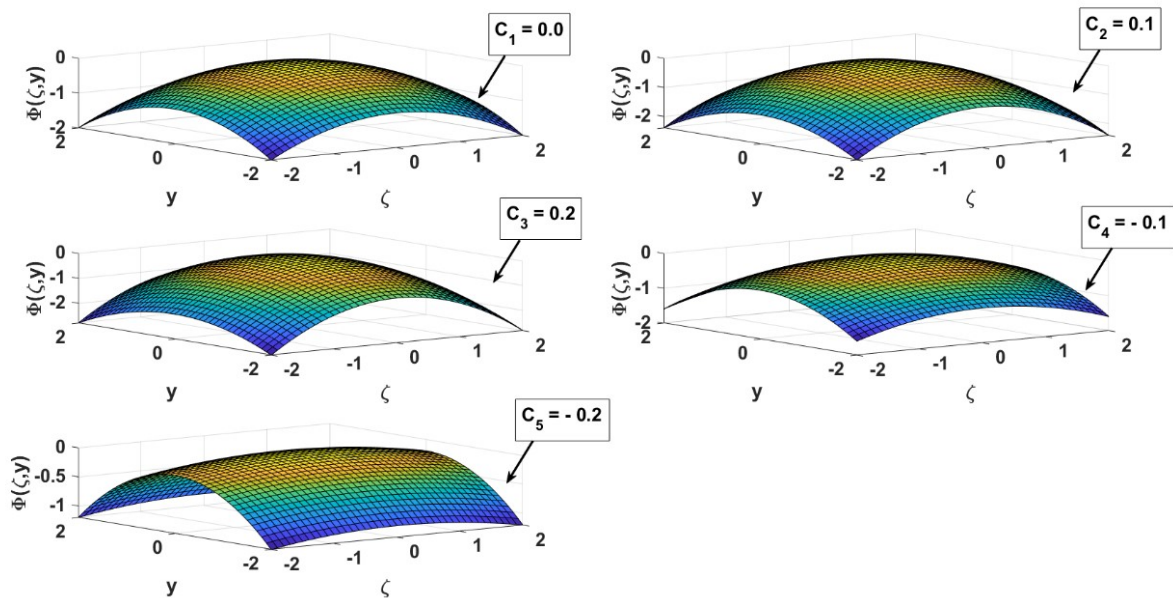
Figure 2. Variation of geometrical parameter η^2 along y-direction related to shape of bubble having residual electrons density n_a along x-direction with a change of transverse geometrical coefficient C.

2.1 $A_x = \phi$ and wakefield potential $\Phi = A_x + \phi$

The simplified d'Alembert equations can be written as (Appendix)

$$\nabla_\perp^2 \Phi = -(1 - v_b^2)\frac{\partial^2 \Phi}{\partial \zeta^2} + \frac{2}{1 - v_b}(n_a - 1 - n_a v_b v_x) \quad (16)$$

$$\nabla_\perp^2 \mathbf{A}_\perp + (1 - v_b^2)\frac{\partial^2 \mathbf{A}_\perp}{\partial \zeta^2} = \nabla_\perp(\frac{1 - v_b}{2}\frac{\partial \Phi}{\partial \zeta} + \nabla_\perp.\mathbf{A}_\perp) \quad (15)$$

$$\frac{\partial^2 \Phi}{\partial \zeta^2} = \frac{2(n_a - 1 - n_a v_x)}{(1 - v_b)^2} - \frac{2}{1 - v_b}\frac{\partial}{\partial \zeta}(\nabla_\perp.\mathbf{A}_\perp) \quad (17)$$
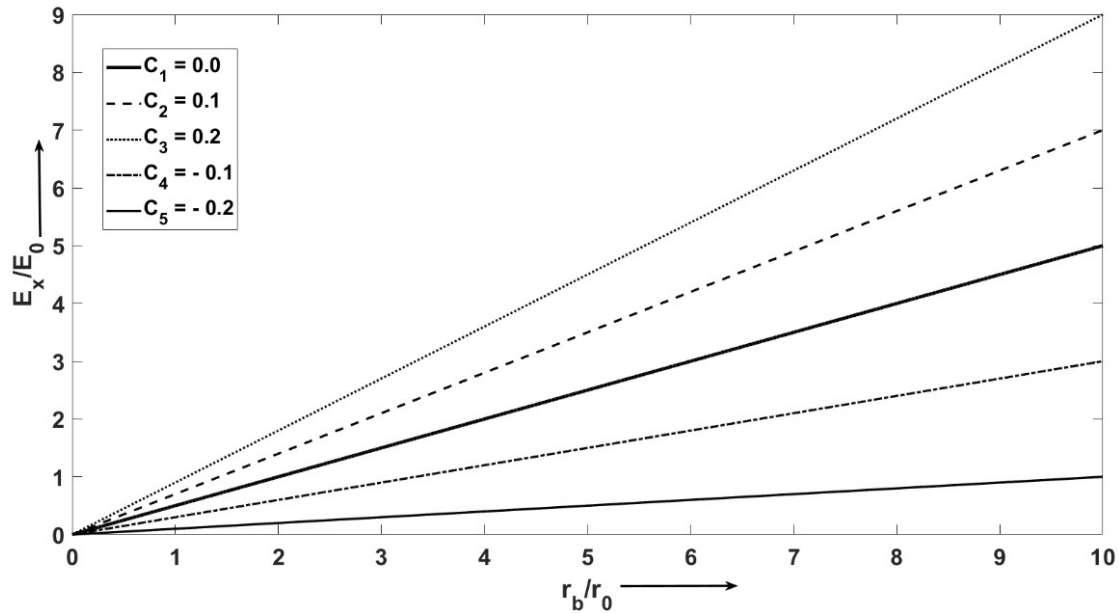
Figure 3. Variation of accelerating field or wakefield E_x with bubble radius r_b along the propagation direction with different values of transverse geometrical coefficient.
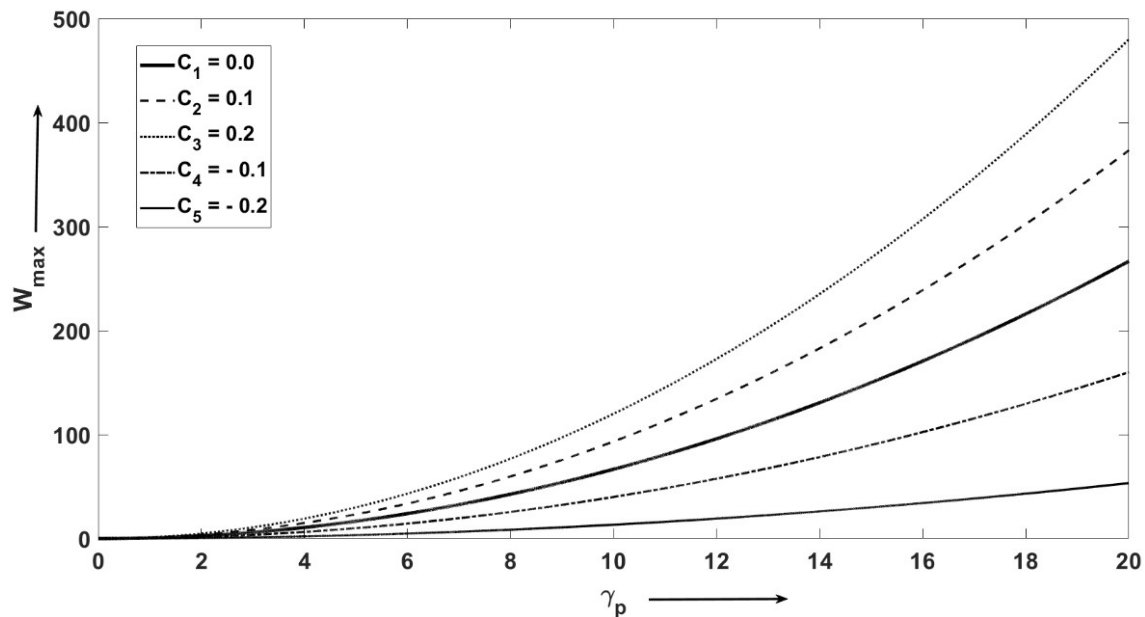
Figure 4. Variation of maximum energy gain W_{max} with relativistic Lorentz factor γ_p along the x-direction for different values of geometrical coefficient C.

From 15 and 16, we can find

$$\nabla_\perp^2 \mathbf{A}_\perp + (1 - v_b^2)\frac{\partial^2 \mathbf{A}_\perp}{\partial \zeta^2} = 0 \qquad (18)$$

General solutions of this equation can be written as

$$\mathbf{A}_\perp = C\zeta y\hat{J} + C\zeta z\hat{k} \qquad (19)$$

$$\Phi = \frac{\zeta^2}{a^2} + \frac{y^2 + z^2}{b^2} \qquad (20)$$

Here a, b and C are the coefficients that control the geometry of the bubble. Using 15 - 18 we find:
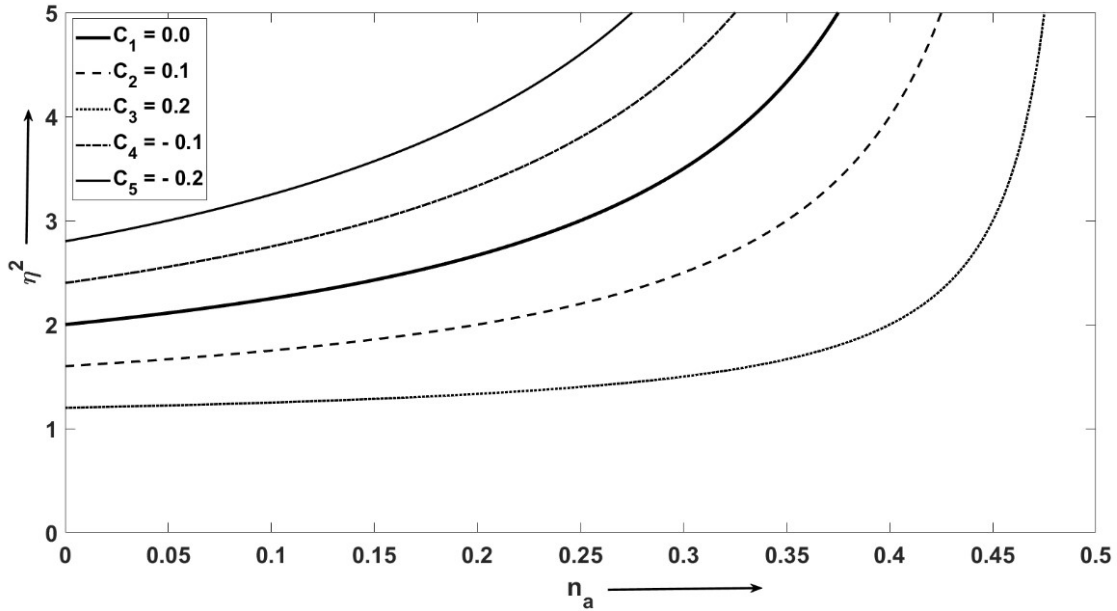
Figure 5. Variation of geoemtrical parameter η^2 as a function of residual electrons density n_a for different transverse coefficient C.
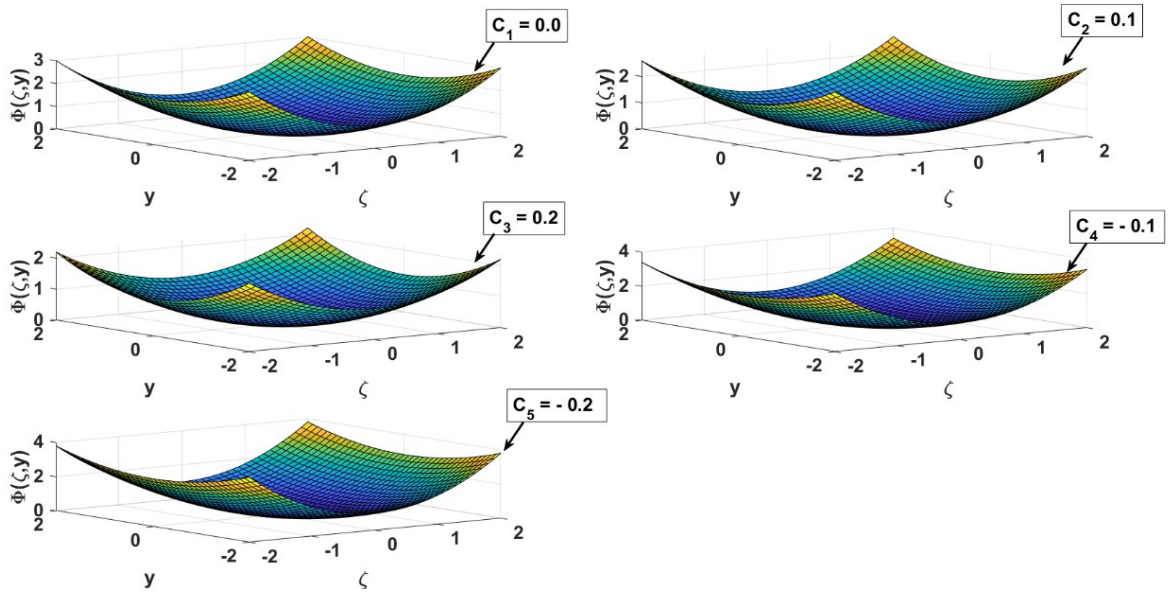
Figure 6. Variation of wakefield potential $\Phi = (\frac{1}{2} - C)\zeta^2 + \frac{y^2}{4}$ as a function of (ζ, y) direction with changing of transverse coefficient C.

$$\frac{1}{a^2} = \frac{(n_a - 1 - n_a v_x)}{(1 - v_b)^2} - \frac{2C}{1 - v_b} \qquad (21)$$

$$\frac{2}{b^2} = -\frac{(1 - v_b^2)}{a^2} + \frac{(n_a - 1 - n_a v_b v_x)}{1 - v_b} \qquad (22)$$

2.2 Bubble geometry

For bubble geometry, following parameter is defined

$$\eta^2 = \frac{b^2}{a^2} = \frac{2}{1 - v_b}$$

$$\frac{(n_a - 1 - n_a v_x) - 2C(1 - v_b)}{(n_a - 1 - n_a v_b v_x) - (1 + v_b) \cdot [n_a - 1 - n_a v_x - 2C(1 - v_b)]} \qquad (23)$$
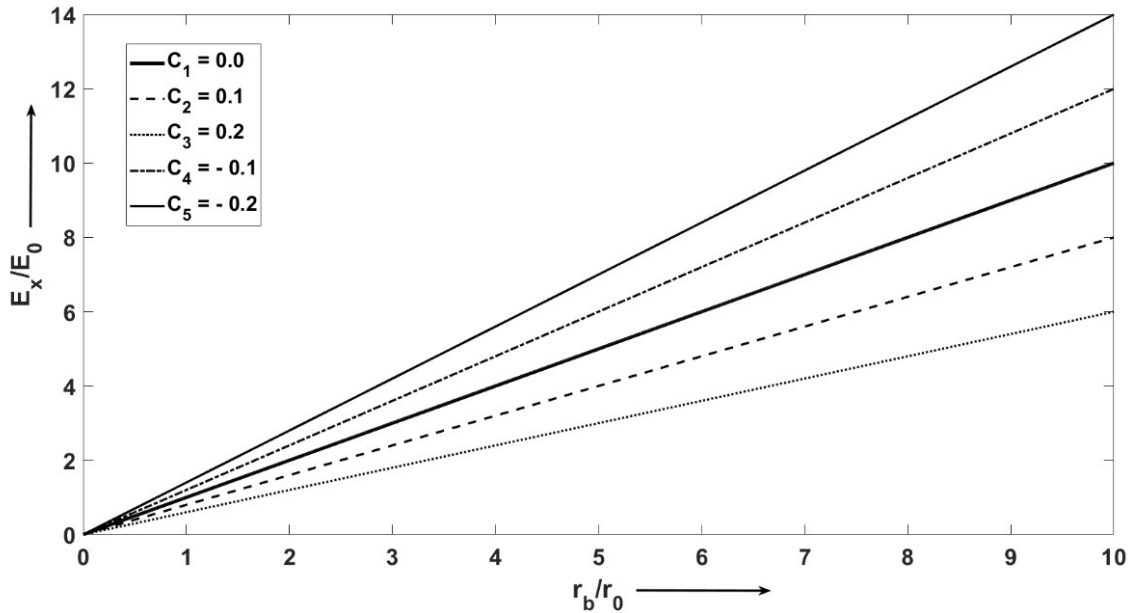
Figure 7. Variation of accelerating field or wakefield E_x as a function of bubble radius r_b along propagation direction x, for different values of transverse geometrical coefficient C.

Here, b is transverse parameter and a is longitudinal parameter and for $b > a$ then $\eta > 1$, bubble transforms into transverse ellipsoid bubble and $b < a$ then $\eta < 1$, bubble transforms into longitudinal ellipsoid bubble and for $b = a$, $\eta = 1$, spherical bubble is formed. For $v_x = 1$, $v_b = -1$

$$\eta^2 = \frac{1 + 4C}{1 - 2n_a} \tag{24}$$

Bubble shape transformation depends upon two parameters, one is geometrical coefficient and other is variation of residual electron density. Here, residual electrons play important role for changing bubble shape. If we consider positive value of geometrical coefficient C, bubble initially is transverse ellipsoid and if we increase the value of residual electron density, bubble shape changes to longitudinal ellipsoid.

If we change the value of geometrical coefficient C, then the shape of the bubble is changed. For example, $C_1 = 0$ gives spherical bubble (1). The deviation from the spherical shape starts with the finite values of C. For the positive values of C, the shape changes from spherical to longitudinal (please see graphs for $C_2 = 0.1$ and $C_3 = 0.2$). On the other hand, transverse ellipsoid bubble is obtained for lower value of C (please see graphs for $C_4 = -0.1$ and $C_5 = -0.2$).

3. Wakefield potential in different shaped bubble regime

From 20, wakefield potential is

$$\Phi = \frac{\zeta^2}{a^2} + \frac{y^2 + z^2}{b^2}$$

and we have used

$$\Phi = \frac{\zeta^2}{a^2} + \frac{y^2}{b^2} \qquad z = 0$$

For $v_x = 1$, $v_b = -1$, $n_a = 0$,

$$\frac{1}{a^2} = -\frac{1}{4} - C, \frac{1}{b^2} = -\frac{1}{4} \tag{25}$$

$$\Phi = \left(-\frac{1}{4} - C\right)\zeta^2 - \frac{y^2}{4} \tag{26}$$

Wakepotential profile is shown in Fig.2 for different values of C. Consistent to the variation of parameters η^2, the wakepotential also turns from spherical to longitudinal ellipsoid or transverse ellipsoid in accordance with the positive and negative values of C, respectively. Wakefield potential changes from spherical at $C_1 = 0$ to longitudinal ellipsoid potential at $C_2 = 0.1$ and at $C_3 = 0.2$ and transverse ellipsoid wakepotential at $C_4 = -0.1$ and at $C_5 = -0.2$ as depicted in Fig.2.

3.1 Electromagnetic field in the bubble regime

From the above equations, we can find all the components of the electromagnetic field

$$E_x = -(1 - v_b)\left(\frac{(n_a - 1 - n_a v_x)}{(1 - v_b)^2} - \frac{2C}{1 - v_b}\right)\zeta \tag{27}$$

$$\frac{E_y}{y} = \frac{E_z}{z} = C(1 + 2v_b) +$$
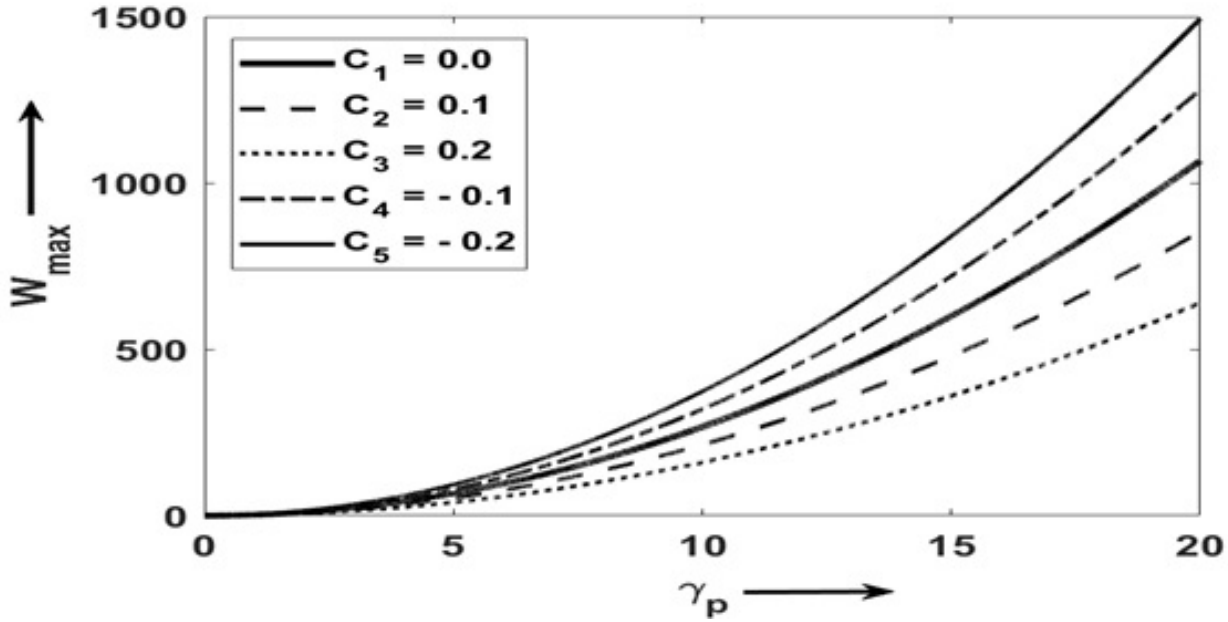
Figure 8. Variation of maximum energy gain W_{max} along y-direction with relativistic Lorentz factor γ_p along x-direction with the change of transverse geometrical coefficient C.

$$\frac{(n_a - 1 - n_a v_b v_x) - (n_a - 1 - n_a v_x)(1 + v_b)}{2(1 - v_b)} \quad (28)$$

and

$$B_x = 0 \quad (29)$$

$$\frac{B_y}{z} = -\frac{B_z}{y} =$$

$$\frac{(n_a - 1 - n_a v_b v_x) - (1 - n_a - n_a v_x)(1 + v_b)}{2(1 - v_b)} + v_b \quad (30)$$

These are for the realistic situation of residual electrons. However, for electron free cavity i.e. when $n_a = 0$ and $v_b = -1$, we have

$$E_x = (\frac{1}{2} + 2C)\zeta$$

$$E_y = (-\frac{y}{4} - Cy)\zeta \quad (31)$$

$$E_z = (-\frac{z}{4} - Cz)$$

and

$$B_x = 0$$

$$B_y = (-\frac{z}{4} - Cz) \quad (32)$$

$$B_z = (\frac{y}{4} + Cy)$$

3.2 Acceleration gradient

From equation 31, we analyze longitudinal and transverse electric and magnetic fields, but acceleration of electrons takes place by longitudinal electric field. The transverse fields produce radiation due to transverse oscillation of the electrons. Here we focus on the longitudinal electric field in view of the particle acceleration.

Since acceleration occurs at the front side of the bubble, then, $\zeta = r_b$ and the longitudinal electric field

$$E_x = (\frac{1}{2} + 2C)r_b \quad (33)$$

A clear cut variation of field E_x or the acceleration gradient within the bubble is shown in Fig.3 through the variation of bubble radius. The field increases linearly with the longitudinal direction and bigger bubble is supposed to create larger field and hence, the larger accelerator gradient. Corresponding to Figs.1 and 2, i.e. values of C, we notice that the field or gradient in transverse ellipsoid bubble regime for $C_1 = 0.1$ and $C_2 = 0.2$ are more than spherical at $C_1 = 0$ and longitudinal ellipsoid bubble regime at $C_4 = -0.1$ and $C_5 = -0.2$.

3.3 Maximum energy gain

Based on the expressions of the electric field E_x and dephasing length L_d, we calculate the maximum energy gain, as

$$W_{max} = E_x L_d \quad (34)$$

$$W_{max} = (\frac{1 + 4C}{3})a_0 \gamma_p^2 \quad (35)$$
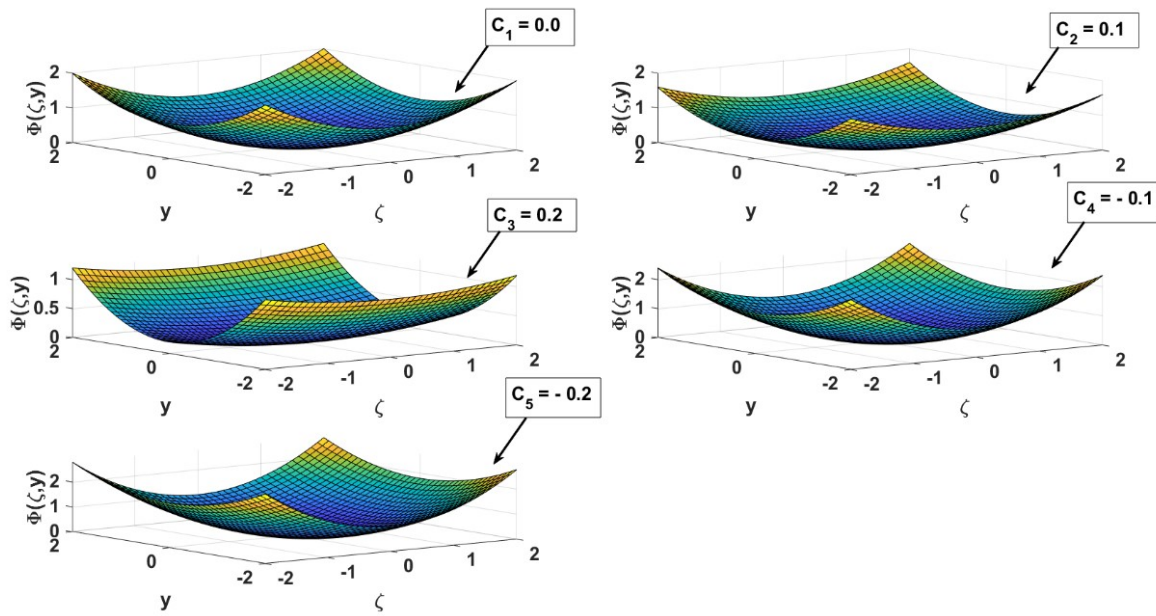
Figure 9. Variation of wakefield potential $\Phi = (\frac{1}{4} - C)\zeta^2 + \frac{y^2}{4}$ along (ζ, y) direction with changing of transverse coefficient C.
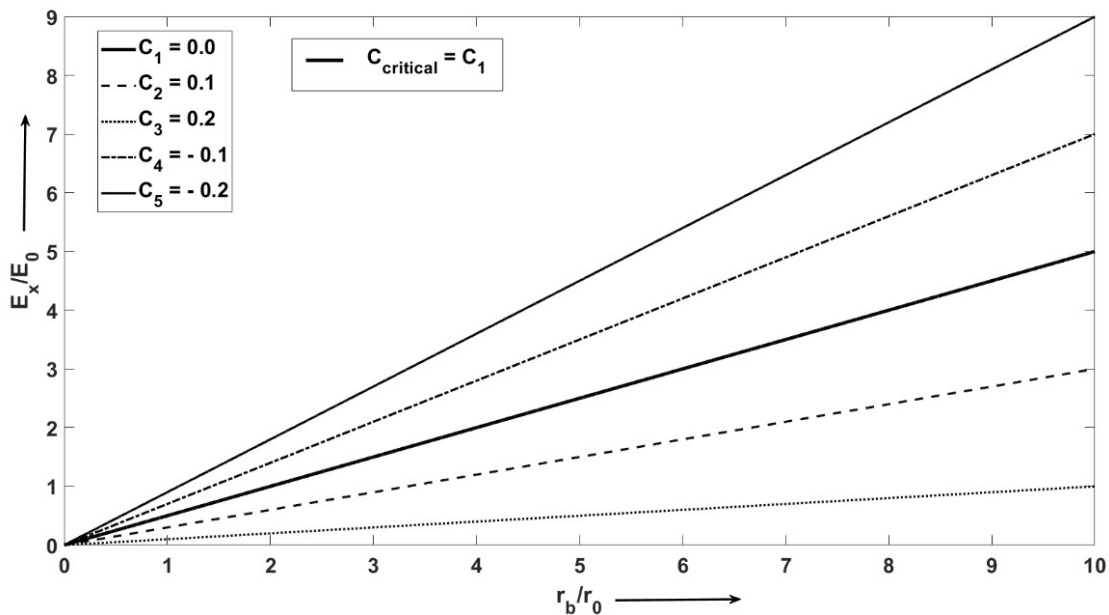
Figure 10. Variation of accelerating field or wakefield E_x along y – direction with bubble radius r_b along propagation direction x- axis with the change of transverse geometrical coefficient C.

The dependence of maximum energy gain on the Lorentz factor and shape of bubble is shown in Fig.4 through the variation of γ_p and C. As expected maximum energy gain becomes higher and higher with the increase in the Lorentz factor and attains value > 12. In this region, the maximum energy increases almost exponentially with γ_p. On the other hand, the maximum energy gain is more in transverse ellipsoid bubble at $C_2 = 0.1$ and $C_3 = 0.2$ than that of spherical bubble at $C_1 = 0$ and longitudinal ellipsoid bubble regime at $C_4 = -0.1$ and $C_5 = -0.2$ for the laser strength parameter $a_0 = 2$. If we consider higher value of a_0 then wakefield is not uniform and for higher value of a_0, density of plasma electrons should be higher but this case is for overdense plasma. With present value of electron density, bubble or nonlinear regime has been made but for higher value of a_0, this regime does not occur with this situation.
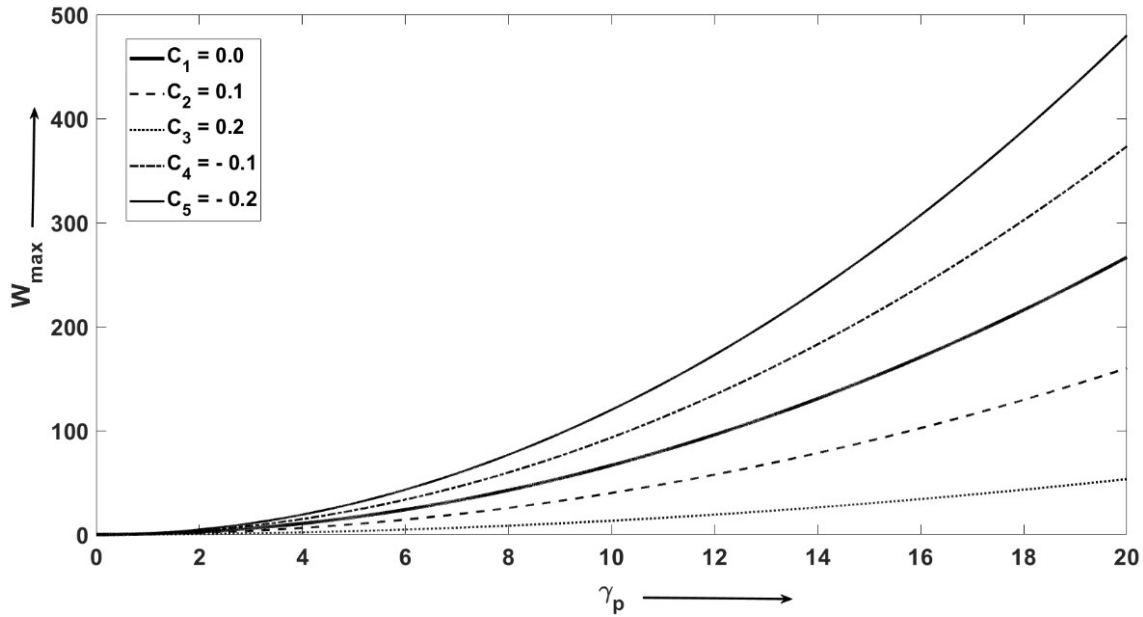
Figure 11. Variation of maximum energy gain W_{max} along y-direction with relativistic Lorentz factor γ_p along x-direction with the change of transverse geometrical coefficient C.

4. $\nabla_\perp . \mathbf{A}_\perp = -\frac{\partial \phi}{\partial \zeta}$, $\Phi = A_x - \phi$

The d'Alembert equations in this case can be written as

$$\nabla_\perp^2 \mathbf{A}_\perp + (1 - v_b^2)\frac{\partial^2 \mathbf{A}_\perp}{\partial \zeta^2} = \nabla_\perp(\frac{\partial \Phi}{\partial \zeta} - v_b\frac{\partial \phi}{\partial \zeta}) \quad (36)$$

$$\nabla_\perp^2 \Phi + v_b(1 - v_b)\frac{\partial^2 \Phi}{\partial \zeta^2} + v_b(1 - v_b)\frac{\partial^2 \phi}{\partial \zeta^2} = 1 - n_a + n_a v_x \quad (37)$$

$$\frac{\partial^2 \phi}{\partial \zeta^2} + \nabla_\perp^2 \phi - v_b\frac{\partial^2 \Phi}{\partial \zeta^2} = n_a - 1 \quad (38)$$

Solutions of 34, 35 and 36 are 19, 20

$$\phi(\zeta, y, z) = -C\zeta^2 + K(y^2 + z^2)/4 \quad (39)$$

together with

$$K = n_a - 1 + 2C + \frac{2v_b}{a^2} \quad (40)$$

$$\frac{1}{a^2} = \frac{1}{2v_b}(1 - n_a + K - 2C) \quad (41)$$

$$\frac{4}{b^2} = [1 - n_a + n_a v_x + 2Cv_b(1 - v_b) -$$

$$(1 - v_b)(1 - n_a + K - 2C)] \quad (42)$$

$$\eta^2 = \frac{b^2}{a^2} =$$

$$\frac{2(1 - n_a + K - 2C)}{v_b[1 - n_a + n_a v_x + 2Cv_b(1 - v_b) - (1 - v_b)(1 - n_a + K - 2C)]} \quad (43)$$

4.1 Bubble geometry

For $K = 0$, $C \neq 0$, $n_a \neq 0$, $v_b = 1$, $v_x = -1$, the geometrical parameter is obtained as

$$\eta^2 = \frac{2 - 2n_a - 4C}{1 - 2n_a} \quad (44)$$

With the consideration of $\nabla_\perp \cdot \mathbf{A}_\perp = -\frac{\partial \phi}{\partial \zeta}$, $\Phi = A_x - \phi$, it is seen that the geometrical shape of bubble changes only in transverse ellipsoid shape for different values of geometrical coefficient C (6). Wakefield potential changes from spherical at $C_1 = 0$ to longitudinal ellipsoid potential at $C_2 = 0.1$ and at $C_3 = 0.2$ and transverse ellipsoid wake-potential at $C_4 = -0.1$ and at $C_5 = -0.2$.

4.2 Wakefield potential

For $K = 0$, $C \neq 0$, $n_a \neq 0$, $v_b = 1$, $v_x = -1$

$$\Phi = (0.5 - C)\zeta^2 + 0.25y^2 \quad (45)$$

4.3 Acceleration gradient

$$E_x = 2C\zeta(1 - v_b) + 2\zeta v_b \frac{1 - n_a + K - 2C}{2v_b} \tag{46}$$

For $v_b = 1$, $\zeta = r_b$, $K = 0$

$$E_x = r_b(1 - n_a - 2C) \tag{47}$$

For $n_a = 0$,
Figure 7 shows the variation of field E_x or the acceleration gradient with the radius of bubble for different values of geometrical parameter r_b. Clearly larger field or gradient is realized in a bigger size bubble. Moreover, acceleration field in transverse ellipsoid bubble regime for $C_4 = -0.1$ and $C_5 = -0.2$ stays larger than the case of spherical bubble at $C_1 = 0$ and longitudinal ellipsoid bubble at $C_2 = 0.1$ and $C_3 = 0.2$. For all the cases, the field stays larger than the previous case of different Gauge conditions.

4.4 Maximum energy gain

Using the same concept as discussed in previous section, we find the maximum energy gain as

$$W_{max} = E_x L_d = \frac{4}{3}(1 - n_a - 2C)a_0 \gamma_p^2 \tag{48}$$

For $n_a = 0$, it reads

$$W_{max} = \frac{4}{3}(1 - 2C)a_0 \gamma_p^2 \tag{49}$$

Figure 8 makes a comparative study of the maximum energy gain for different values of geometrical coefficient and Lorentz factor. However, the gain is much larger in the present case (Please see Fig.4 for comparison). With regard to the importance of shape of the bubble for maximum energy gain, it can be observed that the energy is more in transverse ellipsoid bubble at $C_2 = 0.1$ and at $C_3 = 0.2$ than that of spherical bubble at $C_1 = 0$ and longitudinal ellipsoid bubble regime at $C_4 = -0.1$ and $C_5 = -0.2$ with laser pulse strength $a_0 = 2$.

5. Special case

In order to uncover the role of Gauge selection for realizing appreciable acceleration of electrons, we also compare our results with the ones obtained by Li et al. [10] for the Gauge $A_x = -\phi$ and wakefield potential $\Phi = A_x - \phi$

$$\Phi = (\frac{1}{4} - C)\zeta^2 + \frac{r^2}{4} \tag{50}$$

The shape of this wakefield potential is shown in Fig.9. Here also we see that the change in potential profile in view of different values of C.

5.1 Electromagnetic field in bubble regime

In addition, we calculate the longitudinal electric field E_x that is important for the electron acceleration. This is given as

$$E_x = (1 + v_b)(\frac{(1 - n_a - n_a v_x)}{(1 + v_b)^2} - \frac{2C}{1 + v_b})\zeta \tag{51}$$

For $v_x = -1$, $v_b = 1$, $\zeta = r_b$, $n_a = 0$, this reads

$$E_x = (\frac{1}{2} - 2C)\zeta = (\frac{1}{2} - 2C)r_b \tag{52}$$

This field (or the acceleration gradient) is plotted in Fig.**??** for different size/radius of bubble and geometrical parameter. The behaviour of E_x remains the same as discussed for the previous cases of Gauge conditions. However, the magnitude remains different. Similar is the case with maximum energy gain, $W_{max} = (\frac{2 - 8C}{3})a_0 \gamma_p^2$ as shown in Fig 11. A comparative study of Figs.3, 7 and 10 shows that the electric field is the largest for the Gauge condition $\nabla_\perp . A_\perp = -\frac{\partial \phi}{\partial \zeta}$ and $\Phi = A_x - \phi$. This Gauge condition also stays the best with respect to the maximum energy gain (please see Figs. 4, 8 and 11)
In order to solve the present problem of bubble wakefield acceleration, we used an analytical approach. However, such a system of equations can also be solved numerically. The numerical and simulation approaches have proved to be very effective in different areas [29–32]. The other interesting part of the present work could be see the role of laser pulse shapes which have proved to be efficient for the THz radiation generation [33–35] and interesting nonlinear phenomena in optics [36, 37].

6. Conclusion

Geometrical shape of bubble in bubble wakefield acceleration mechanism changes to transverse, spherical, and longitudinal ellipsoid depending on different Gauges conditions and the wakefield potential assumes spherical to longitudinal and transverse ellipsoid profiles. The calculations show that the energy gain limited by dephasing length yields its maximum value in transverse ellipsoid bubble than that of spherical and longitudinal ellipsoid bubbles in each Gauge condition. In particular energy gain is found to be greater for $\nabla_\perp . A_\perp = -\frac{\partial \phi}{\partial \zeta}$, $\Phi = A_x - \phi$ than $A_x = -\phi$, $\Phi = A_x - \phi$ and $A_x = \phi$, $\Phi = A_x + \phi$ cases.

References

[1] T. Tajima and J.M. Dawson. *Phys. Rev. Lett.*, **43**:266, 1979.

[2] E.S. Toosi, S. Mirzanejhad, and D .Dorranian. *Laser Part. Beams*, **34**:193, 2016.

[3] H.K. Malik, S. Kumar, and Y. Nishida. *Opt. Commun.*, **280**:417, 2007.

[4] H.K. Malik, S.Kumar, and K.P. Singh. *Laser Part. Beams*, **26**:197, 2008.

[5] K. Nakajima, A. Enomoto, H. Kobayashi, H. Nakanishi, Y. Nishida, A. Ogata, S. Ohsawa, T. Oogoe, T. Shoji, and T. Urano. *Nucl. Instruments Methods Phys. Res. Sect. A Accel. Spectrometers, Detect. Assoc. Equip.*, **292**:12, 1990.

[6] Y. Golian and D. Dorranian. *J. Theor. Appl. Phys.*, **11**:27, 2017.

[7] H.K. Malik. *J. Appl. Phys.*, **104**:53308, 2008.

[8] D.K. Singh, J.R. Davies, G. Sarri, F. Fiuza, and L.O. Silva. *Phys. Plasmas.*, **19**:73111, 2012.

[9] S. Hakimi, N. Beier, Y. Ma, J. Hinojosa, A. Hussein, A. Maksimchuk, J. Nees, T. Tajima, K. Krushelnick, and A. Thomas. *APS Division of Plasma Physics Meeting Abstracts. pp. GP*, **20**:12, 2012.

[10] M.S. Bloom, M.J.V. Streeter, S. Kneip, R.A. Bendoyro, O. Cheklov, J.M. Cole, A. Döpp, C.J. Hooker, J. Holloway, and J. Jiang. *Phys. Rev. Accel. Beams.*, **23**:61301, 2020.

[11] H.P. Schlenvoigt, K. Haupt, A. Debus, F. Budde, O. Jäckel, S. Pfotenhauer, H. Schwoerer, E. Rohwer, J.G. Gallacher, E. Brunetti, R.P. Shanks, S.M. Wiggins, and D.A. Jaroszynski. *Nat. Phys.*, **14**:130–133, 2008.

[12] S. Barzegar and A.R. Niknam. *Sci. Rep.*, **11**:1–8, 2021.

[13] W. Lu, C. Huang, M. Zhou, M. Tzoufras, F.S. Tsung, W.B. Mori, and T. Katsouleas. *Phys. Plasmas.*, **13**:56709, 2006.

[14] M.W. Lin, C.Y. Hsieh, D.K. Tran, and S.H. Chen. *Phys. Plasmas.*, **27**:13102, 2020.

[15] M.W. Lin, T.Y. Chu, Y.Z. YChen, D.K. Tran, H.H. Chu, S.H. Chen, and J. Wang. *Phys. Plasmas.*, **27**:113102, 2020.

[16] D. Woodbury, A. Korolov, R. Schwartz, and H. Milchberg. *APS Division of Plasma Physics Meeting Abstracts.*, **7**:008, 2018.

[17] D. Seipt Y. Ma, S.J.D. Dann, M.J.V. Streeter, C.A.J. Palmer, L. Willingale, and A.G.R. Thomas. *Phys. Plasmas.*, **25**:113105, 2018.

[18] R. Dhawan and H.K. Malik. *Chinese J. Phys.*, **66**:560–572, 2020.

[19] R. Dhawan and H.K. Malik. *Vacuum*, **177**:109354, 2020.

[20] R. Dhawan, M. Kumar, and H.K. Malik. *Phys. Plasmas.*, **27**:63515, 2020.

[21] I. Kostyukov, A. Pukhov, and S. Kiselev. *Phys. Plasmas.*, **11**:5256–5264, 2004.

[22] H.C. Wu, B.S. Xie, S. Zhang, X.R. Hong, X.Y. Zhao, and M.P. Liu. *Phys. Plasmas.*, **17**:113103, 2010.

[23] R. Sadighi-Bonabi and S.H. Rahmatollahpur. *Phys. Plasmas.*, **71**:33105, 2010.

[24] X.F. Li, Q. Yu, Y.J. Gu, S. Huang, Q. Kong, and S. Kawata. *Phys. Plasmas.*, **22**:83112, 2015.

[25] J. Wood. *ethos.bl.uk*, **30**:739605, 2016.

[26] E. Esarey and M. Pilloff. *Phys. Plasmas.*, **2**:1432–1436, 1995.

[27] E. Esarey, C.B. Schroeder, and W.P. Leemans. *Rev. Mod. Phys.*, **81**:1229, 2009.

[28] W. Lu, M. Tzoufras, C. Joshi, F.S. Tsung, W.B. Mori, J. Vieira, R.A. Fonseca, and L.O. Silva. *Phys. Rev. Spec. Top. Beams.*, **10**:61301, 2007.

[29] L. Malik and A. Tevatia. *Def. Sci. J.*, **17**:518, 2021.

[30] L. Malik, S. Rawat, M. Kumar, and A. Tevatia. *Mater. Today Proc.*, **38**:191–197, 2021.

[31] L. Malik, A. Escarguel, M. Kumar, A. Tevatia, and R.S. Sirohi. *Laser Phys. Lett.*, **18**:86003, 2021.

[32] L. Malik, M. Kumar, and I.V. Singh. *IEEE Trans. Plasma Sci.*, **49**:2227–2237, 2021.

[33] H.K. Malik. *Laser-Matter Interaction for Radiation and Energy*. CRC Press, 1th edition, 2021.

[34] H.K. Malik. *Phys. Lett. A.*, **384**:126304, 2020.

[35] R. Gill, D. Singh, and H.K. Malik. *J. Theor. Appl. Phys.*, **11**:103–108, 2017.

[36] L. Malik and A. Escarguel. *Europhysics Letters*, **124**:64002, 2019.

[37] L. Malik. *Opt. Laser Technol.*, **132**:106485, 2020.

Appendix

d'Alembert equations: Under the quasi-static approximation, all the quantities depend on $\zeta = x - v_b t$. Hence, L.H.S. of Eq. 12 reads

$$\frac{\partial}{\partial \zeta}(\nabla_\perp . \mathbf{A}_\perp) - \nabla_\perp^2 A_x$$

for *x* direction, and

$$\nabla_\perp(\nabla_\perp . \mathbf{A}_\perp) + \nabla_\perp(\frac{\partial A_x}{\partial \zeta}) - \nabla_\perp^2 \mathbf{A}_\perp - \frac{\partial^2 \mathbf{A}_\perp}{\partial \zeta^2}$$

for *y* and *z* directions.
Combining L.H.S. and R.H.S. of Eq. 12, we get

$$\frac{\partial}{\partial \zeta}(\nabla_\perp . \mathbf{A}_\perp) - \frac{1}{2}\nabla_\perp^2 \Phi = -n_a v_x + \frac{v_b}{2}\frac{\partial^2 \Phi}{\partial \zeta^2} - \frac{v_b^2}{2}\frac{\partial^2 \Phi}{\partial \zeta^2}$$

for *x* direction and

$$\nabla_\perp(\nabla_\perp . \mathbf{A}_\perp) + \frac{1}{2}\nabla_\perp(\frac{\partial \Phi}{\partial \zeta}) - \nabla_\perp^2 \mathbf{A}_\perp - \frac{\partial^2 \mathbf{A}_\perp}{\partial \zeta^2} =$$

$$\frac{v_b}{2}\nabla_\perp(\frac{\partial \Phi}{\partial \zeta}) - \frac{v_b^2}{2}\frac{\partial^2 \mathbf{A}_\perp}{\partial \zeta^2}$$

for *y* and *z* directions with $J_x = -n_a v_x$ and $\mathbf{J}_\perp = 0$, after solving Eqs. (15) and (11), we find

$$\frac{\partial^2 \Phi}{\partial \zeta^2} = \frac{2(n_a - 1 - n_a v_x)}{(1 - v_b)^2} - \frac{2}{1 - v_b}\frac{\partial}{\partial \zeta}(\nabla_\perp . \mathbf{A}_\perp)$$

for x direction.

For perpendicular directions

$$\nabla_\perp^2 \Phi = 1(1 - v_b^2)\frac{\partial^2 \Phi}{\partial \zeta^2} + \frac{2}{1/v_b}(n_a - 1 - n_a v_b v_x)$$

From Eqs. 15 and 12, we find;

$$\nabla_\perp^2 \mathbf{A}_\perp + (1 - v_b^2)\frac{\partial^2 \mathbf{A}_\perp}{\partial \zeta^2} = \nabla_\perp(\frac{1 - v_b}{2}\frac{\partial \Phi}{\partial \zeta} + \nabla_\perp.\mathbf{A}_\perp)$$